

Plasmonic nanolaser for intracavity spectroscopy and sensorics

P. Melentiev, A. Kalmykov, A. Gritchenko, A. Afanasiev, V. Balykin, A. S. Baburin, E. Ryzhova, I. Filippov, I. A. Rodionov, I. A. Nechepurenko, A. V. Dorofeenko, I. Ryzhikov, A. P. Vinogradov, A. A. Zyablovsky, E. S. Andrianov, and A. A. Lisyansky

Citation: *Appl. Phys. Lett.* **111**, 213104 (2017);

View online: <https://doi.org/10.1063/1.5003655>

View Table of Contents: <http://aip.scitation.org/toc/apl/111/21>

Published by the [American Institute of Physics](#)

Articles you may be interested in

[A broadband metasurface Luneburg lens for microwave surface waves](#)

Applied Physics Letters **111**, 211603 (2017); 10.1063/1.5003571

[Spectrally resolved surface plasmon resonance dispersion using half-ball optics](#)

Applied Physics Letters **111**, 201102 (2017); 10.1063/1.4999636

[Electronic control of linear-to-circular polarization conversion using a reconfigurable metasurface](#)

Applied Physics Letters **111**, 214101 (2017); 10.1063/1.4998556

[High-efficiency and low-loss gallium nitride dielectric metasurfaces for nanophotonics at visible wavelengths](#)

Applied Physics Letters **111**, 221101 (2017); 10.1063/1.5007007

[Dual-surface flexible THz Fano metasensor](#)

Applied Physics Letters **111**, 201101 (2017); 10.1063/1.5000428

[Wideband metamaterial array with polarization-independent and wide incident angle for harvesting ambient electromagnetic energy and wireless power transfer](#)

Applied Physics Letters **111**, 213902 (2017); 10.1063/1.4986320

Scilight

Sharp, quick summaries **illuminating**
the latest physics research

Sign up for **FREE!**

AIP
Publishing

Plasmonic nanolaser for intracavity spectroscopy and sensorics

P. Melentiev,^{1,a)} A. Kalmykov,^{1,2} A. Gritchenko,^{1,3} A. Afanasiev,¹ V. Balykin,^{1,a)}
 A. S. Baburin,^{4,6} E. Ryzhova,^{4,6} I. Filippov,^{4,6} I. A. Rodionov,^{4,6,a)} I. A. Nechepurenko,⁶
 A. V. Dorofeenko,^{3,5,6} I. Ryzhikov,^{3,5} A. P. Vinogradov,^{3,5,6} A. A. Zyablovsky,⁶
 E. S. Andrianov,^{3,6} and A. A. Lisyansky^{7,8,a)}

¹*Institute of Spectroscopy RAS, Troitsk, Moscow 142190, Russia*

²*National Research University, Higher School of Economics, Moscow 101000, Russia*

³*Moscow Institute of Physics and Technology, Dolgoprudny 141700, Russia*

⁴*Bauman Moscow State Technical University, Moscow 105005, Russia*

⁵*Institute for Theoretical and Applied Electromagnetics RAS, Moscow 125412, Russia*

⁶*Dukhov Research Institute of Automatics, Moscow 127055, Russia*

⁷*Department of Physics, Queens College of the City University of New York, Queens, New York 11367, USA*

⁸*The Graduate Center of the City University of New York, New York, New York 10016, USA*

(Received 6 September 2017; accepted 3 November 2017; published online 21 November 2017)

We demonstrate intracavity plasmonic laser spectroscopy using a plasmonic laser created from a periodically perforated silver film with a liquid gain medium. An active zone of the laser is formed by a highly elongated spot of pumping. This results in a significantly more efficient diffusive mixing of dye molecules, which suppresses the effect of their bleaching, and in the ability to reduce the volume of the gain medium to as little as 400 nl. We use this design for a stable plasmonic laser in multiple measurements and demonstrate that it is highly effective as a spaser spectroscopy sensor for intracavity detection of an absorptive dye at 0.07 ppm. This work provides an opportunity to develop applications of intracavity plasmonic laser spectroscopy in biological label detection and other fields. © 2017 Author(s). All article content, except where otherwise noted, is licensed under a Creative Commons Attribution (CC BY) license (<http://creativecommons.org/licenses/by/4.0/>).

<https://doi.org/10.1063/1.5003655>

In laser physics, intracavity laser spectroscopy methods are known to have an extremely high sensitivity.¹ In these methods, an analyte is placed in the laser cavity. This analyte should absorb at the lasing wavelength. As a consequence, the analyte is detected by changing the lasing parameters, such as the threshold, lasing intensity, and wavelength. Usually, it manifests in an appearance of dips in the lasing spectrum.

The dynamics of a plasmonic laser, or spaser, shares many characteristics with that of a traditional laser.^{2–7} Plasmonic laser intracavity spectroscopy was first proposed theoretically.^{8–10} In particular, it has been shown that, similar to conventional intracavity laser spectroscopy, the use of plasmonic lasers can lead to an increase in the efficiency of plasmonic sensors by up to two orders of magnitude.⁸

Different successful experimental approaches have been recently reported.^{11–13} In these studies, a spaser based on CdSe and CdS crystals of micronic size has been sunk into the surrounding medium; an addition of an analyte to that medium results in the modification of the spaser generation frequency^{11,12} or intensity.¹³ Particularly, in Ref. 13, as opposed to conventional intracavity spectroscopy, an addition of an analyte results in an increase in gain, and as a consequence, the laser intensity is boosted.

In this study, we deal with the conventional approach in the sensor design, in which an addition of an analyte is assumed to decrease the intensity of radiation. To begin

with, we design a *planar plasmonic laser*, extending the idea and implementation of plasmonic lasers reported elsewhere.^{14–22} We use a liquid gain medium and a perforated metallic film. The use of this “flow-through” liquid gain enables the direct introduction of an analyte into the active region that warrants both the maximal sensitivity and multiple usage of the sensor. We expect that the subwavelength scale of the plasmonic cavity and the employment of microfluidics make plasmonic intracavity spectroscopy suitable for lab-on-chip technology.²³

It seems that for the design of a plasmonic laser, the greater gain the better. However, it has been recently shown that dye molecules are optimal for plasmonic lasers because the usage of quantum wells with greater gain results in energy loss via spontaneous emission.²⁴ Moreover, the dye molecules are capable of nearly 100% yield and allow for the creation of an optically homogeneous medium with high gain.²⁵

The main shortcoming of this type of active medium is photobleaching, in which a dye molecule is unable to continue fluorescence after approximately 10^5 – 10^6 photon emissions.²⁶ In other words, in the CW regime, a laser using dye in a polymer matrix lives for only 1 ms.

In this paper, we describe an implementation of a pulsed pumped plasmonic laser that uses a *solution* of R101 dye in dimethyl sulfoxide (DMSO) as the gain medium. The pulse duration and energy should be small enough so that photobleaching does not occur. The pumping should be sufficient to saturate the excitation of dye molecules. The experiment shows that the required pump power is about 1 MW/cm². Such pumping causes bleaching of dye molecules in 100

^{a)}Authors to whom correspondence should be addressed: melentiev@isan.troitsk.ru; balykin@isan.troitsk.ru; irodionov@bmsu.ru; and alexander.lisyansky@qc.cuny.edu

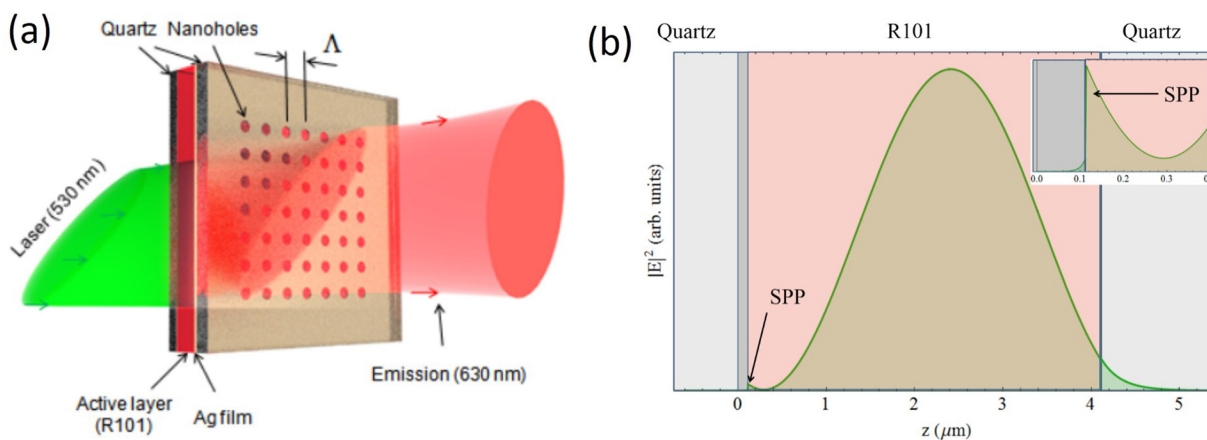


FIG. 1. Planar plasmonic laser. (a) The laser apparatus using a perforated silver film. (b) The spatial distribution of the electric field intensity of the TM polarized mode in the quartz/silver (100 nm)/DMSO (1000 nm)/quartz system. The inset shows the electric field near the silver/DMSO interface.

μs .²⁶ Thus, the pump pulse duration should be shorter than this value.

The use of a liquid gain medium offers a number of advantages over a solid gain medium by fixing the bleaching problem. In a DMSO solution, dye molecules diffuse for a distance of $l \approx \sqrt{2Dt}$ with the diffusion coefficient $D \approx 0.1 \text{ cm}^2/\text{s}$. In our experimental setup, the size of the pumped region is about $0.1 \text{ cm} \times 0.002 \text{ cm}$. A dye molecule diffuses for a distance of $l = 0.002 \text{ cm}$ per $2.0 \times 10^{-5} \text{ s}$ that determines the repeating frequency of $5 \times 10^4 \text{ Hz}$. Using any frequency smaller than $5 \times 10^4 \text{ Hz}$ ensures that each pulse interacts with new dye molecules. Therefore, photobleaching is highly suppressed, and a temporarily stable gain medium is formed.

Figure 1(a) shows the setup used in this study. It is a planar waveguide made of a liquid DMSO layer deposited on a plasmonic crystal. The plasmonic crystal is formed by an array of nanoholes created in a 100-nm-thin silver film deposited onto a quartz substrate. The optimal parameters of the plasmonic crystal have been numerically calculated. To compensate the uncertainty in the calculated values of the material parameters, we fabricated and studied structures with nanoholes of the varying pitch Λ (545, 555, 565, 575, and 585 nm) and the diameter (150, 175, and 200 nm).

The nanohole arrays in the silver films are fabricated by electron-beam lithography and dry etching. As shown in Fig. 2, the array of holes is patterned on a $100 \pm 5 \text{ nm}$ thick silver film, which is deposited on a UV-grade quartz substrate with a roughness of the order of 1 nm. The silver film is deposited by electron-beam evaporation with a base pressure of $5 \times 10^{-8} \text{ Torr}$, and then, it is capped by a 10-nm-layer of SiO_2 . The process for silver film electron-beam evaporation on quartz substrate is developed as the part of the detailed study of silver film formation mechanisms.²⁷ The quality of the silver films is monitored by scanning electron microscopy (SEM) and electron backscatter diffraction (EBSD), yielding an average film grain size of about $1 \mu\text{m}$ (see Fig. 3), as well as by stylus profilometry, yielding an rms roughness of less than 1.2 nm, and by spectroscopic ellipsometry, which results in optical properties similar to those reported in Ref. 28. Although making an array of nanoholes with electron-beam lithography creates defects in the

silver film and diminishes the grain size down to several dozen nanometers, it does not affect the quality of the nanoholes (Fig. 2). The use of the SiO_2 -film solves two issues: It suppresses the silver degradation and prevents the quenching of excited dye molecules. The quenching leads to an undesirable heating of the silver film, which, in turn, leads to sample destruction at pumping intensities above $2 \text{ MW}/\text{cm}^2$.

Since the losses in silver are large, we deal with hybrid modes. In principle, the optimal lasing parameters are obtained when the bulk of the mode energy is contained in the DMSO layer with dye molecules. In this study, we experimentally determine that for lasing, the minimal possible gain layer thickness should be $4 \mu\text{m}$. The calculated field distribution in the TM mode is shown in Fig. 1(b). Hybridization between the photonic and plasmonic modes is maximal at the DMSO/metal interface.

The gain medium is formed by the solution of the R101 dye in DMSO with the concentration of $6 \times 10^{18} \text{ cm}^{-3}$. This system provides a material gain near 75 cm^{-1} via pulsed optical pumping at the wavelength of 530 nm. To decrease the threshold pumping, we have chosen a specific geometry of the pumping beam, which selectively excites some modes. In particular, the pumping region takes the form of an extended ellipse with the major and minor axes equal to 1.6 mm and $20 \mu\text{m}$, respectively. Comparing to the commonly used circular pumping region with the same diameter as the major axis of the ellipse of this geometry, our approach leads to an $80\times$ -increase in the intensity of the light pumping of the dye molecules, and consequently, the

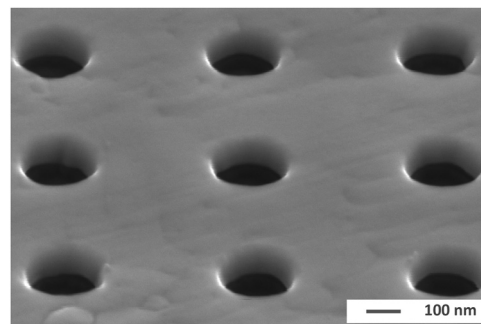


FIG. 2. SEM images of an array of 200 nm nanoholes with a pitch of 565 nm fabricated in a silver film.

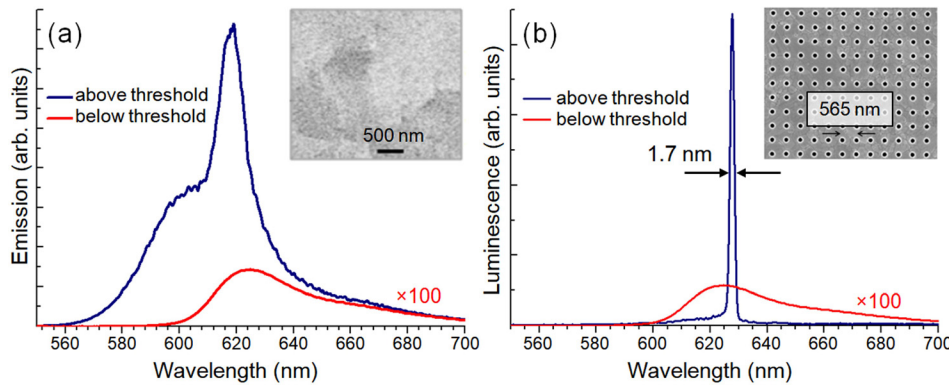


FIG. 3. Measured radiation spectra of different samples. (a) The spectrum of dye luminescence in the quartz/silver/DMSO/quartz system without nano-holes, with radiation output through a defect in the form of the 5- μ m-wide slit passing through the film. (b) The luminescence spectrum of the plasmonic laser. The pump levels below and above threshold correspond to 0.09 and 0.9 MW/cm², respectively. The insets show electronic microscopy images of the samples.

power of the pumping laser can be decreased. The major axis is aligned along the 1.4 mm diagonal of the nanohole array. Therefore, 0.1 mm of the pumped region lies outside of the nanohole array on each side. The peak pumping strength is varied up to the value of 5 MW/cm², significantly exceeding the saturation intensity of the R101 optical transition.

We use the repeating frequency of 40 Hz with a pulse duration of 10 ns. Such a value of the repeating frequency is much smaller than the estimation of 5×10^4 Hz given above; therefore, during the time between pulses, the diffusion of dye molecules ensures their replacement in the working volume. The volume of the gain medium in the pumped region is four orders of magnitude smaller than the volume of the total gain medium. This leads to a long-lived stable generation regime that can be sustained for several weeks (the sample was subjected to repeated pulsed pumping for 2 h each day for two weeks; no degradation of the gain medium was observed) with the use of only 400 nl of the gain medium.

In order to characterize the system, the spectrum of dye luminescence is initially measured for the system without nano-holes. Radiation is brought out through a slit in the metal film with the width of about 2 μ m. In Fig. 3(a), one can see the change in the luminescence spectrum depending on the pumping level. This change demonstrates a threshold behavior. At low pumping, below the threshold, the luminescence spectrum of the sample coincides with that of a single R101 dye molecule. It has a maximum at 620 nm and the spectral width at half-maximum being equal to 40 nm. Above the threshold, at high pumping (>0.9 MW/cm²), a narrower, 12 nm, spectral line centered at 618 nm emerges. Such a narrowing line and the presence of the threshold are characteristics of the multimode amplified spontaneous emission (ASE).²⁹

Next, we consider the situation when the elongated pumping spot covers the area greater than the perforated area of the silver film in the (1,1)-direction. The boundaries between the solid surface and the perforated area form a resonator. The eigenmodes of this resonator are formed by the reflection of the hybrid waves from these boundaries. This reflection is due to the difference in impedances of these waves in perforated and non-perforated areas. Although the reflectance of the hybrid waves is small, it is sufficient for lasing.

The smallest lasing threshold, which we observed, occurs for the sample with the square array of 175 nm nano-holes and has a pitch of 565 nm. The spectrum of the

plasmonic laser is measured in the far field with the peak intensity at the angle of $\theta = 5^\circ$.

A wave propagating over a periodically perforated surface is a Bloch wave comprised of harmonics with wavevectors $\{k_x - n_x g_x, k_y - n_y g_y\}$, where $k_x = k_y = k_t/\sqrt{2}$, n_x and n_y are integers, $k_t = k_0 n_{eff}$, $1.46 < n_{eff} < 1.475$, and $g_x = g_y = 2\pi/L$. In our case, the only leaky harmonic $\left(\sqrt{(k_x - n_x g_x)^2 + (k_y - n_y g_y)^2} < k_0\right)$ is the one with $n_x = n_y = 1$. Its angle of radiation is $\theta = \arcsin\left[\sqrt{(k_x - n_x g_x)^2 + (k_y - n_y g_y)^2}/k_0\right] \approx 5.8^\circ$, which is in agreement with the experiment.

The experimental spectra of dye luminescence for two values of pumping are shown in Fig. 3(b). At intensities below 500 kW/cm², the spectral contour is very similar to that of usual R101 dye luminescence. However, at higher (above 500 kW/cm²) pumping intensities, the luminescence contour changes dramatically, and a very narrow spectral line with the half-width of 1.7 nm emerges at 628 nm. Such a narrow linewidth indicates that we deal not with amplified spontaneous emission (ASE) but with lasing.³⁰

Figure 4 shows the dependence of the lasing intensity and the spectral width on the pumping strength obtained in the experiment. These measurements are carried out by imaging the microscope focal plane onto the CCD camera by means of a Bertrand lens.³¹ We observe a threshold behavior of plasmonic laser radiation with the threshold pumping value of 500 kW/cm² corresponding to a gain coefficient of ~ 40 cm⁻¹.

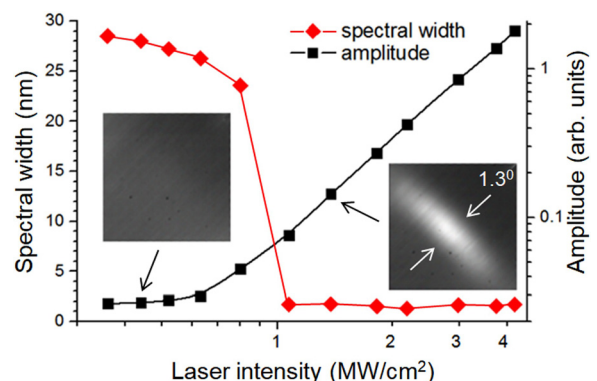


FIG. 4. Generation intensity and linewidth dependence of the plasmonic laser. Insets show the angular distribution of the intensity in the radiation pattern for pumping intensities below and above the lasing threshold.

The insets in Fig. 4 show the dependence of the angular radiation distribution of the plasmonic laser for pumping intensities below and above the threshold. Above the plasmonic lasing threshold, directional radiation is observed. The radiation pattern is extended in the direction perpendicular to the extension direction of the pumping region. The minimal directivity is $\sim 1.3^\circ$; however, in the orthogonal direction, it is 4.1° .

Let us demonstrate the possibility of applying the plasmonic laser in sensing and intracavity spectroscopy.^{8–10} The apparatus is shown in the inset of Fig. 5. We start with the R101 solution in DMSO with the concentration of 700 ppm. We use the cyanine-5 dye, which has a broad absorption band around the lasing spectral region, as the analyte. We prepare mixed solutions of R101 and cyanine-5 dye in DMSO. While the concentration of R101 is 700 ppm, we use three concentrations, 7, 0.7, and 0.07 ppm, of cyanine-5. Before cyanine-5 is injected via a microfluidic input, the gain medium without cyanine-5 dye has been removed from the lasing cavity. We use the solution volume of 800 nl, twice than that of the dye solution above the nanohole array. Therefore, the measurement at each analyte concentration requires an extremely small probe volume, which is a principal feature of our sensor.

The resulting lasing curves are shown in Fig. 5. In addition to the lasing suppression by the absorptive dye, we detect a minimal concentration of 70 ppb, thereby proving the ultra-high detection sensitivity of our novel scheme. This concentration corresponds to the theoretical estimates of the detection limit based on the dye absorption cross-section. The results presented in Fig. 5 show that the output power of the plasmonic nanolaser is sensitive to the analyte concentration in a nonlinear way. This may happen because the Cy-5 spectral absorption profile differs from the active medium spectral amplification profile. Adding the analyte solution into the plasmonic nanolaser not only decreases the output intensity but also changes the spectral shape of the gain. As a result, the wavelength of lasing may change as well.

We implement and study the plasmonic laser generation based on hybrid modes of a plasmonic crystal and a photonic waveguide interacting with the gain medium of R101 dye

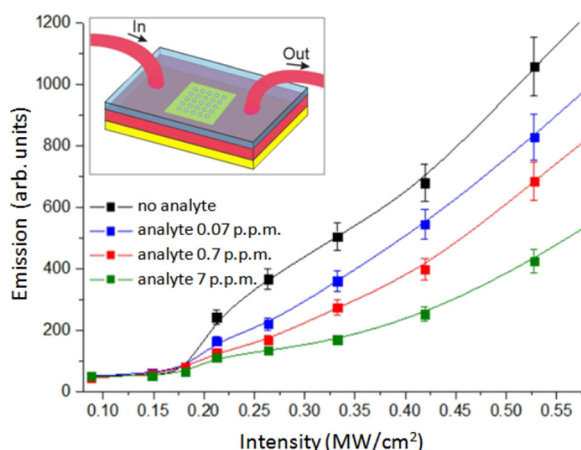


FIG. 5. Lasing intensity vs. pumping rate at different cyanine-5 dye concentrations in the lasing cavity. The sketch of the experimental setup is shown in the inset.

solution. The laser cavity is formed by a nanohole array in a silver film. The threshold behavior of the radiation characteristics with an increase in the pump power is demonstrated along with the high directivity above the threshold. The plasmonic laser cavity is characterized by an ultra-low loss (40 cm^{-1}) owing to the use of an ultra-high-quality silver film and the hybrid plasmonic-photonic mode. Lasing at 628 nm, with a linewidth of 1.7 nm and a directivity of 1.3° , is observed. Based on the implemented scheme, we also demonstrate a possibility of intracavity plasmonic laser spectroscopy using an analyte concentration of 70 ppb.

We would like to thank Yu. Lozovik, Yu. Vainer, R. Gordon, A. Schokker, F. Koenderink, and A. Kalatskiy for helpful discussions. This research was supported by the Advanced Research Foundation (Contract No. 7/004/2013-2018) and Russian Foundation for Basic Research (Grant No. 17-02-01093). Samples were made at the BMSTU Nanofabrication Facility (Functional Micro/Nanosystems, FMNS REC, ID 74300). A.A.L. acknowledges support from the NSF under Grant No. DMR-1312707.

¹V. M. Baev, T. P. Belikova, E. A. Sviridenkov, and A. F. Suchkov, *Sov. Phys. JETP* **47**, 21–29 (1978).

²D. J. Bergman and M. I. Stockman, *Phys. Rev. Lett.* **90**, 027402 (2003).

³M. I. Stockman, *Nat. Photonics* **2**, 327–329 (2008).

⁴M. A. Noginov, G. Zhu, A. M. Belgrave, R. Bakker, V. M. Shalaev, E. E. Narimanov, S. Stout, E. Herz, T. Suteewong, and U. Wiesner, *Nature* **460**, 1110–1112 (2009).

⁵M. I. Stockman, *Phys. Rev. Lett.* **106**, 156802 (2011).

⁶A. A. Lisyansky, I. A. Nechepurenko, A. V. Dorofeenko, A. P. Vinogradov, and A. A. Pukhov, *Phys. Rev. B* **84**, 153409 (2011).

⁷E. S. Andrianov, A. A. Pukhov, A. V. Dorofeenko, A. P. Vinogradov, and A. A. Lisyansky, *Phys. Rev. B* **85**, 035405 (2012).

⁸Y. E. Lozovik, I. Nechepurenko, and A. Dorofeenko, *Photonics Nanostruct. Fundam. Appl.* **21**, 60–66 (2016).

⁹Y. E. Lozovik, I. Nechepurenko, A. Dorofeenko, E. Andrianov, and A. Pukhov, *Laser Phys. Lett.* **11**, 125701 (2014).

¹⁰Y. E. Lozovik, I. A. Nechepurenko, A. V. Dorofeenko, E. S. Andrianov, and A. A. Pukhov, *Phys. Lett. A* **378**, 723–727 (2014).

¹¹X.-Y. Wang, Y.-L. Wang, S. Wang, B. Li, X.-W. Zhang, L. Dai, and R.-M. Ma, *Nanophotonics* **6**, 472–478 (2017).

¹²S. Wang, B. Li, X.-Y. Wang, H.-Z. Chen, Y.-L. Wang, X.-W. Zhang, L. Dai, and R.-M. Ma, *ACS Photonics* **4**, 1355–1360 (2017).

¹³R.-M. Ma, S. Ota, Y. Li, S. Yang, and X. Zhang, *Nat. Nano.* **9**, 600–604 (2014).

¹⁴M. J. Marell, B. Smalbrugge, E. J. Geluk, P. J. van Veldhoven, B. Barcones, B. Koopmans, R. Nötzel, M. K. Smit, and M. T. Hill, *Opt. Express* **19**, 15109–15118 (2011).

¹⁵F. van Beijnum, P. J. van Veldhoven, E. J. Geluk, M. J. A. de Dood, G. W. 't Hooft, and M. P. van Exter, *Phys. Rev. Lett.* **110**, 206802 (2013).

¹⁶A. V. Dorofeenko, A. A. Zyablovsky, A. P. Vinogradov, E. S. Andrianov, A. A. Pukhov, and A. A. Lisyansky, *Opt. Express* **21**, 14539–14547 (2013).

¹⁷X. Meng, J. Liu, A. V. Kildishev, and V. M. Shalaev, *Laser Photonics Rev.* **8**, 896–903 (2014).

¹⁸A. H. Schokker and A. F. Koenderink, *Phys. Rev. B* **90**, 155452 (2014).

¹⁹A. H. Schokker and A. F. Koenderink, *ACS Photonics* **2**, 1289–1297 (2015).

²⁰W. Zhou, M. Dridi, J. Y. Suh, C. H. Kim, D. T. Co, M. R. Wasielewski, G. C. Schatz, and T. W. Odom, *Nat. Nanotechnol.* **8**, 506–511 (2013).

²¹P. Molina, E. Yraola, M. O. Ramirez, C. Tserkezis, J. L. Plaza, J. Aizpurua, J. B. Abad, and L. E. Bausa, *Nano Lett.* **16**, 895–899 (2016).

²²T. Hakala, H. Rekola, A. Väkeväinen, J.-P. Martikainen, M. Nečada, A. Moilanen, and P. Törmä, *Nat. Commun.* **8**, 13687 (2017).

²³O. Tokel, U. H. Yildiz, F. Inci, N. G. Durmus, O. O. Ekiz, B. Turker, C. Cetin, S. Rao, K. Sridhar, and N. Natarajan, *Sci. Rep.* **5**, 9152 (2015).

²⁴A. A. Zyablovsky, I. A. Nechepurenko, E. S. Andrianov, A. V. Dorofeenko, A. A. Pukhov, A. P. Vinogradov, and A. A. Lisyansky, *Phys. Rev. B* **95**, 205417 (2017).

²⁵M. T. Hill and M. C. Gather, *Nat. Photonics* **8**, 908–918 (2014).

- ²⁶R. Zondervan, F. Kulzer, M. A. Kol'chenk, and M. Orrit, *J. Phys. Chem. A* **108**, 1657–1665 (2004).
- ²⁷A. S. Baburin, A. R. Gabidullin, A. V. Zverev, I. A. Rodionov, I. A. Ryzhikov, and Y. V. Panfilov, *Herald Bauman Moscow State Tech. Univ. Instrum. Eng.* No. 6, 4–14 (2016).
- ²⁸P. B. Johnson and R.-W. Christy, *Phys. Rev. B* **6**, 4370 (1972).
- ²⁹S. Murai, Y. Tokuda, K. Fujita, and K. Tanaka, *Appl. Phys. Lett.* **101**, 031117 (2012).
- ³⁰P. Berini and I. De Leon, *Nat. Photonics* **6**, 16–24 (2012).
- ³¹L. Wang, A. S. Shorokhov, P. N. Melentiev, S. Kruk, M. Decker, C. Helgert, F. Setzpfandt, A. A. Fedyanin, Y. S. Kivshar, and D. N. Neshev, *ACS Photonics* **3**, 1494–1499 (2016).